Developing and characterizing MR/CT-visible materials used in QA phantoms for MRgRT systems

Angela Steinmann[a)]
Department of Radiation Physics, The University of Texas M. D. Anderson Cancer Center, Houston, TX 77030, USA

R. Jason Stafford
Department of Imaging Physics, The University of Texas M. D. Anderson Cancer Center, Houston, TX 77030, USA

Gabriel Sawakuchi, Zhifei Wen, and Laurence Court
Department of Radiation Physics, The University of Texas M. D. Anderson Cancer Center, Houston, TX 77030, USA

Clifton D. Fuller
Department of Radiation Oncology, The University of Texas M. D. Anderson Cancer Center, Houston, TX 77030, USA

David Followill
Department of Radiation Physics, The University of Texas M. D. Anderson Cancer Center, Houston, TX 77030, USA

(Received 24 May 2017; revised 21 August 2017; accepted for publication 5 October 2017; published 21 December 2017)

Purpose: Synthetic tissue equivalent (STE) materials currently used to simulate tumor and surrounding tissues for IROC-Houston's anthropomorphic head and thorax QA phantoms cannot be visualized using magnetic resonance (MR) imaging. The purpose of this study was to characterize dual MR/CT-visible STE materials that can be used in an end-to-end QA phantom for MR-guided radiotherapy (MRgRT) modalities.

Methods: Over 80 materials' MR, CT, and dosimetric STE properties were investigated for use in MRgRT QA phantoms. The materials tested included homogeneous and heterogeneous materials to simulate soft tissue/tumor and lung tissues. Materials were scanned on a Siemens' Magnetom Espree 1.5 T using four sequences, which showed the materials visual contrast between T1- and T2-weighted images. Each material's Hounsfield number and electron density data was collected using a GE's CT Lightspeed Simulator. Dosimetric properties were examined by constructing a $10 \times 10 \times 20$ cm^3 phantom of the selected STE materials that was divided into three sections: anterior, middle, and posterior. Anterior and posterior pieces were composed of polystyrene, whereas the middle section was substituted with the selected STE materials. EBT3 film was inserted into the phantom's midline and was irradiated using an Elekta's Versa 6 MV beam with a prescription of 6 Gy at 1.5 cm and varying field size of: 10×10 cm^2, 6×6 cm^2, and 3×3 cm^2. Measured film PDD curves were compared to planning system calculations and conventional STE materials' percent depth dose (PDD) curves.

Results: The majority of the tested materials showed comparable CT attenuation properties to their respective organ site; however, most of the tested materials were not visible on either T1- or T2-weighted MR images. Silicone, hydrocarbon, synthetic gelatin, and liquid PVC plastic-based materials showed good MR image contrast. In-house lung equivalent materials made with either silicone- or hydrocarbon-based materials had HUs ranging from: −978 to −117 and −667 to −593, respectively. Synthetic gelatin and PVC plastic-based materials resembled soft tissue/tumor equivalent materials and had HUs of: −175 to −170 and −29 to 32, respectively.

PDD curves of the selected MR/CT-visible materials were comparable to IROC-Houston's conventional phantom STE materials. The smallest field size showed the largest disagreements, where the average discrepancies between calculated and measured PDD curves were 1.8% and 5.9% for homogeneous and heterogeneous testing materials, respectively.

Conclusions: Gelatin, liquid plastic, and hydrocarbon-based materials were determined as alternative STE substitutes for MRgRT QA phantoms. [https://doi.org/10.1002/mp.12700]

Key words: anthropomorphic QA phantoms, MRgRT, MRI -guided radiotherapy

1. INTRODUCTION

Advances in radiation oncology have drastically evolved over the past decade. Among the many changes, one of the most prominent additions is the use of onboard imaging in conjunction with a radiation therapy treatment modality (i.e., cone-beam CT-guided linear accelerator). While the integration of cone-beam CT (CBCT) with a modern linear accelerator enables patient set-up verification and target localization, this imaging modality is often limited to interfraction set-up

verifications.[1–3] Several research collaborations were initiated several years ago to integrate a magnetic resonance imager (MR) with either a ^{60}Co unit or a linear accelerator as a new form of image-guided radiation therapy.[2,4] In comparison with CBCT, the integrated MR can provide images with superior soft tissue contrast, permit real-time imaging, and not cause any additional radiation dose. The incorporation of a magnetic resonance-guided radiation therapy (MRgRT) modality into the clinic can provide visualization for both intrafractional and interfractional target motion.

In the United States, there are two MRgRT systems: the Unity developed by Elekta/Philips (Elekta, Crawley, United Kingdom and Philips, Amsterdam, Netherlands) which is not yet in clinical use and the ViewRay MRIdian (ViewRay, Oakwood Village, OH, USA) which is in clinical use. The Unity system is equipped with an Elekta 7 MV linear accelerator that is located in between a Philips' 1.5 T MR scanner. Due to the active shielding on the superconducting magnets, a low magnetic field toroid is created, which enables a linear accelerator to be positioned and operate in between the two magnets with only a minimal magnetic effect.[5,6] In contrast, the MRIdian is a radiation therapy (RT) treatment machine with three independent ^{60}Co sources located in between a split 0.35 T superconducting MR imager.[7] Each of the three ^{60}Co treatment heads is equipped with a double-focused multileaf collimator; thus, permitting the MRIdian unit to have a comparable penumbra and dose rate as a conventional 6 MV linear accelerator.[7] Additionally, ViewRay has developed a linac-based version of the MRIdian system. The MRIdian Linac, which was FDA approved in February 2017, is an upgraded system that incorporates a 0.35 T superconducting magnetics with a 6 MV linear accelerator.

Both MRgRT systems have the ability to provide real-time imaging and deliver adaptive RT. Despite the innovation and potential benefits of using a MR unit for MRgRT treatments, there are challenges that limit a MR-only RT workflow. Two of these include: (a) the inability to easily determine the patient's electron density for treatment planning dose calculations and (b) geometric distortions produced on MR images.[8–12] Conventionally, the patient's electron density is indirectly determined through a bi-linear relationship between the linear attenuation data collected from a CT and the material's respectively density. Unlike CT, where images are created from back projections of photons penetrating the body, MR does not use radiation to produce an image and solely relies on small fluctuations of the materials' net magnetic moment. Due to the inherent differences in the acquisition process of MR and CT, the linear attenuation data are not collected in MR. Therefore, current MR scanners are unable to indirectly measure electron density from one scan. Additionally, it is critical to know the exact size and location of a patient's anatomy in RT. MR images commonly misrepresent actual patient anatomy in space (geometric distortion) due to the inherent configuration and design of a MR unit.[13] Nonlinear gradients and heterogeneities in the static magnetic field primarily contribute to geometric distortions in the image.[10,12,13] Since geometric distortions and electron densities are limited to the inherent differences in the acquisition process between MR and CT, it is critical that current MRgRT modalities rely on both CT and MR for treatment planning and treatment verification/treatment adaptation, respectively.

End-to-end QA verifications performed for conventional radiation treatments have routinely focused on using a CT imager and a radiotherapy modality. However with the incorporation of MR in radiotherapy, it is important that end-to-end QA tests expand to also include MR imagers. Current end-to-end QA phantoms used at the Imaging and Radiation Oncology Core at Houston (IROC-Houston) QA Center for credentialing purposes in National Cancer Institute (NCI) funded clinical trials are not MR-visible. As shown in Fig. 1, tumor and surrounding tissue in IROC-Houston's anthropomorphic thorax phantom are distinguishable in CT images but are not in T1- and T2-weighted MR images. Dosimetrically, the phantoms are accurate but the plastics used to represent tumor and surround tissue in IROC-Houston's phantoms do not yield any MR signal, which makes these phantoms deficient as end-to-end QA phantoms for MRgRT. Other researchers have attempted to create dual MR/CT phantoms, but the phantoms are limited by either: shelf-life storage, require refrigeration or additives to prevent microorganism growth and therefore were not suitable for shipping to other RT institutions.[14–16]

The aim of this study was to identify and characterize synthetic tissue equivalent (STE) materials that could be used to develop an anthropomorphic dual MR/CT QA phantom which would require minimal maintenance, and be used to credential RT institutions wishing to use MRgRT modalities in NCI-funded clinical trials.

2. MATERIAL AND METHODS

IROC-Houston's two anthropomorphic phantoms used most often are the heterogeneous thorax and homogeneous head and neck (H&N) phantoms. The thorax and H&N phantoms were previously described in detail by Followill and Molineu, respectively.[17,18] Briefly, the current thorax phantom is a water fillable shell and contains two lungs made of compressed cork (one with a centrally located target made of nylon). Other organs at risk represented in IROC-Houston's thorax phantom include a heart and spinal cord composed of polystyrene and acrylic, respectively. In IROC-Houston's H&N phantom, the primary and secondary targets are constructed out of solid water and are surrounded by polystyrene. The polystyrene/solid water insert is enclosed into a water fillable plastic shell, which is shaped as a human head. For both phantoms, the materials used to simulate the targets and surrounding normal tissues are synthetic, rigid, and hydrogen-deficient. These materials are ideal for traditional QA phantoms since they do not require special storage conditions, require minimal maintenance, can easily hold radiation dosimeters, maintain their shape, are distinguishable using CT, and are dosimetrically similar to human tissue.

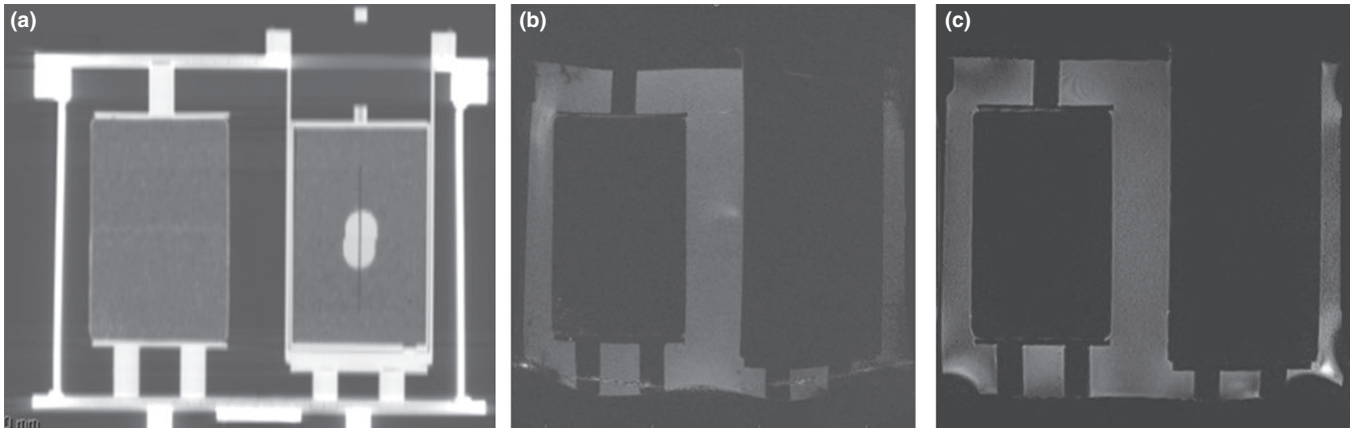

FIG. 1. Images a-c are used to illustrate the need for a dual CT/MR-visible phantom for MRgRT modalities. This figure displays IROC-Houston's Anthropomorphic Thorax phantom imaged in a GE Lightspeed CT simulator (a.) and Siemen's Magnetom Espree 1.5 T MR scanner (b–c). The phantom's tumor and lung were constructed out of polystyrene and compressed cork, respectively. The tumor is located in the phantom's left lung and is completely visible on a CT (a.) however, the tumor and surrounding lung tissue are not visually distinguishable in either a T1-weighted (b.) or T2-weighted (c.) MR image.

To develop an appropriate MRgRT QA phantom, it is vital that the materials used for this dual modality phantom are: (a) visible on both T1- and T2-weighted MR images, (b) visible on CT images, and (c) have comparable HUs and dosimetrically simulate tumor and surrounding tissue. Since IROC-Houston ships their end-to-end QA phantoms to other institutions, these materials must also satisfy nondosimetric characteristics. IROC-Houston's MR/CT-visible materials must also endure rough shipping conditions, show longevity without adding preservatives, maintain their physical structure (i.e., high melting point) and show a relative ease in manipulating the material to form a realistic tissue shape and hold dosimeters. A wide variety of materials (listed in Table I) were tested for their dosimetric, MR and CT compatibility. The materials were first imaged using a MR and CT scanner. Based on the material's MR and CT assessment, a decision was made on what materials to continue with dosimetric testing. Potential materials examined for a MR/CT QA phantom included: nylon-based, silicon-based, acrylic-based, and gel-based materials. In addition to commercially purchased materials, some tested materials were manufactured in-house. The in-house mixtures incorporated mini Styrofoam balls with ranging diameters of 2–4 mm with either a petroleum- or silicone-based material. Combining a based material with Styrofoam balls created a heterogeneous material that could potentially be used to represent a synthetic lung equivalent tissue.

2.A. MR imaging

All materials listed in Table I were submerged in water and were scanned using four MR scanning protocols on a Siemen's Magnetom Espree 1.5 T MR scanner (Siemens Healthcare, Erlangen Germany). Common T1 and T2 MR sequences were chosen based on an assumption that similar sequences would be equipped in all of MRgRT treatment's imaging software. MR scans represented four different MR sequences that were either: (a) currently used in an MRgRT modality (TRUFI) or (b) shared similar sequences (T1-weighted and T2-weighted) that were expected to be equipped in all new MRgRT modalities. All materials were specifically scanned under a TRUFI sequence since ViewRay exclusively uses this sequence.

Four MR sequences, summarized in Table II, were used to image the testing material's MR properties. The water bath was used as a baseline to assess the material's contrast in various MR sequences. A T1-weighted image was obtained from a 3D gradient echo sequence and used the following parameters: FA = 25°, TR = 9.5 ms, TE = 4.68 ms, ETL = 1, NEX = 1. A true fast imaging with steady-state free precession sequence, commonly referred as a TRUFI sequence, was acquired with the following parameters: FA = 70°, TR = 4 ms, TE = 2 ms, ETL = 1, NEX = 1. Two additional T2-weighted images were also obtained for each material. The first T2-weighted image was a gradient sequence and had parameters of: FA = 120°, TR = 3200 ms, TE = 245 ms, ETL = 109, NEX = 2. The second T2-weighted image used a fluid-attenuated inversion recovery sequence, commonly referred as a FLAIR sequence, and had scanning parameters of: FA = 120°, TR = 5000 ms, TE = 336 ms, ETL = 109, NEX = 2.

2.B. CT imaging

All of the materials listed in Table I were submerged in a water bath and were scanned using a brain protocol on a GE Lightspeed CT simulator (General Electric Company, New York, NY, USA). The scanning parameters were: DFOV = 500.0 mm, 120 kVp, 275 mA, and slice thickness = 3 mm. The materials' HU were obtained after exporting the CT images into Philips IntelliSpace PACS Enterprise (Philips, Amsterdam, Netherlands) system.

2.C. Dosimetric properties

A dual MR/CT-visible end-to-end QA anthropomorphic phantom used in radiotherapy must also dosimetrically

TABLE I. Above is a list of materials tested for a MR/CT-visible STE phantom. As displayed in the second column, testing materials were grouped as: plastic, synthetic gelatin, hydrocarbon, urethane, epoxy, silicone, and nylon-based materials. These material's HU were measured from a GE LightSpeed CT Simulator and are displayed in the third column. The materials were also imaged on a Siemen's Magnetom Espree 1.5 MR scanner using T1- and T2-weighted sequences. The fourth and fifth columns display whether the materials could visually be distinguished in T1- and T2-weighted images, respectively. Materials were visualized on a both T1- and T2-weighted sequences, and also shared reasonable HUs for either tumor, soft tissue, and lung materials were then dosimetrically tested. The last column displays whether or not a material was tested dosimetrically. If the material was tested dosimetrically, the final column displays if it was considered STE.

Testing material	Material type	HU	T1-visible	T2- visible	Tissue equivalent
Superflab[a]	Plastic	59.9	Y	Y	Y
SuperStuff[a]	Plastic	65.2	Y	Y	–
100% liquid PVC plastic[b]	Plastic	−10.4	Y	Y	Y
100% super soft PVC plastic[b]	Plastic	3.70	Y	Y	–
90% liquid PVC plastic and 10% plastic softener mix[b]	Plastic	15.7	Y	Y	–
100% plastic hardener[b]	Plastic	32.0	Y	N	–
75% plastic hardener and 25% plastic softener Mix[b]	Plastic	21.9	Y	Y	–
75% Super soft plastic and 25% softener mix[b]	Plastic	−29.7	Y	Y	–
75% liquid PVC plastic and 25% plastic softener mix[b]	Plastic	−6.5	Y	Y	–
Gel #10[c]	Synthetic gelatin	−170	Y	Y	–
Gel #20[c]	Synthetic gelatin	−164	Y	Y	Y
Gel #1[c]	Synthetic gelatin	−169	Y	Y	–
Gel #2[c]	Synthetic gelatin	−172	Y	Y	–
Gel #3[c]	Synthetic gelatin	−171	Y	Y	Y
Gel #4[c]	Synthetic gelatin	−175	Y	Y	–
Multiwax[h]	Hydrocarbon	−156	N	N	–
Petroleum jelly[h]	Hydrocarbon	−154	Y	Y	–
91.7% petroleum jelly and 8.3% Styrofoam ball Mix[i]	In-House hydrocarbon mix	−593	Y	Y	Y
95% petroleum jelly and 5% styrofoam ball Mix[i]	In-House hydrocarbon mix	−667	Y	Y	–
Dragon skin 10[g]	Silicone	262	Y	Y	–
Dragon skin 30[g]	Silicone	294	Y	Y	N
Dragon skin FX-Pro[g]	Silicone	231	Y	Y	–
Eco flex 00-10[g]	Silicone	202	Y	Y	–
EcoFlex 00-30[g]	Silicone	185	Y	Y	–
EcoFlex 00-50[g]	Silicone	203	Y	Y	N
PlatSil® Gel 00[d]	Silicone	275	Y	Y	–
PlatSil® Gel 10[d]	Silicone	319	Y	Y	–
PlatSil® Gel 25[d]	Silicone	290	Y	N	–
PlatSil® Gel 00 + H (10:10:10)[d,◇]	In-House silicone mix	−978	Y	Y	–
PlatSil® Gel 10 + H (10:10:10)[d,◇]	In-house Silicone Mix	−970	Y	Y	–
PlatSil® Gel 25 + H (10:10:10)[d,◇]	In-house silicone mix	−972	Y	N	–
PlatSil® Gel 25 (20:20:0.5)[d,i]	In-house silicone mix	−117	Y	N	–
PlatSil® Gel-00/styrofoam ball mix (20 g:20 g:1 g)[d,i]	In-house silicone mix	−510	Y	Y	–
PlatSil® Gel 25 (20:20:1)[d,i]	In-house silicone mix	−358	Y	N	–
PlatSil® Gel-00/styrofoam ball mix (20 g:20 g:1.5 g)[d,i]	In-house silicone mix	−406	Y	Y	N
PlatSil® Gel 25 (20:20:1.5)[d,i]	In-house silicone mix	−470	Y	N	–
PlatSil® Gel 25 (20:20:2)[d,i]	In-house silicone mix	−494	Y	N	–
PlatSil® Gel-00/Styrofoam ball mix (10 g:10 g:1 g)[d,i]	In-house silicone mix	−655	Y	Y	–
PlatSil® Gel-00/Styrofoam ball mix (40 g:40 g:1 g)[d,i]	In-house silicone mix	−350	Y	Y	N
Nycast ® 6PA- Blue[e]	Nylon	161	N	N	–
Nycast ® 6PA- MoS2 filled[e]	Nylon	94.2	N	N	–
Nycast ® 6PA-Orange[e]	Nylon	99.2	N	N	–
Nycast CP[e]	Nylon	82.7	N	N	–
Nycast Rx[e]	Nylon	90.9	N	N	–
Nylon Nyloil[e]	Nylon	94.2	N	N	–
EP 30[f]	Epoxy	72.9	N	N	–
EP424T[f]	Epoxy	63.0	N	N	–
PMC ® 121/30[g]	Urethane	−10.5	Y	N	–
PMC ® 744[g]	Urethane	−2.90	N	N	–

TABLE I. Continued.

Testing material	Material type	HU	T1-visible	T2- visible	Tissue equivalent
PMC ® 746[g]	Urethane	−11.0	N	N	–
PMC ® 770[g]	Urethane	78.0	N	N	–
PMC ® 790[g]	Urethane	66.1	N	N	–
ReoFlex ® 20[g]	Urethane	−19.5	Y	N	-
ReoFlex ® 30[g]	Urethane	−45.0	Y	N	-
Simpact® 85 A[g]	Urethane	66.0	N	N	-
Simpact® 60 A[g]	Urethane	71.6	N	N	-
VytalFlex® 10[g]	Urethane	−9.0	N	N	-
VytalFlex® 20[g]	Urethane	−18.3	Y	N	-
VytalFlex® 30[g]	Urethane	−27.0	Y	N	-

[a]Radiation Products Design Incorporation, Albertville, MN, USA.
[b]M-F Manufacturing Company, Fort Worth, TX, USA.
[c]Clear Ballistics, Fort Smith, AR, USA.
[d]Polytek® Development Corporation, Easton, PA, USA.
[e]Cast Nylons Limited, Willoughby, OH, USA.
[f]MasterBond, Hackensack, NJ, USA.
[g]Smooth-On Inc., Macungie, PA, USA.
[h]Sonneborn, Parsippany, NJ, USA.
[i]In-house mixture that used % weight of Styrofoam balls from Steve Spangler Science Styrofoam Beads, Englewood, CO, USA.
[◇]PlatSil (R) Part H Hardener by Polytek (R) Development Corporation, Easton, PA, USA.

represent human tissue. Percent depth dose (PDD) curves were obtained to determine the material's dosimetric properties on materials that were MR/CT-visible. As shown in Fig. 2, a 10 cm × 10 cm × 20 cm rectangular phantom was constructed to determine the PDD for selected MR/CT-visible materials. The 20 cm long PDD phantom was divided into three sections: anterior, middle, and posterior, which had lengths of 5.0 cm, 10.0 cm, and 5.0 cm, respectively. The anterior and posterior sections were composed of polystyrene, whereas the middle section was substituted with materials that were visible on both CT and MR. Additionally, two materials commonly used in IROC-Houston's QA phantoms (compress cork and polystyrene) were included in this study to provide controlled PDD curves.

The 6 MV beam from an Elekta Versa HD (Elekta, Stockholm, Sweden) was used to irradiate the PDD phantoms with three different field sizes of: 10 × 10 cm^2, 6 × 6 cm^2, 3 × 3 cm^2. During each irradiation, EBT-3 radiochromic film was inserted into the midline of the PDD phantom. Additional 5 cm of polystyrene was placed around the PDD phantom which ensured proper scatter conditions. Within each field size, the PDD phantom was irradiated three times with a prescribed dose of 600 cGy to d_{max} (d = 1.5 cm).

It was also important to assess how accurate the experimental PDD curves compared to the treatment planning system (TPS). A treatment plan was created among the testing materials for each of the three field sizes. Using Pinnacle's treatment planning (Philips, Amsterdam, Netherlands), the dose from 0.5 to 17.0 cm was calculated and normalized to a depth of 1.5 cm using the collapsed cone dose algorithm. After the films were irradiated, a photoelectron CCD

TABLE II. Four MR scanning parameters were used to visually compare the selected material's contrast between water. Among the parameters, a T1-weighted and T2-weighted sequences were scanned based off of the assumption that other MRgRT systems would have the capability to image basic T1-weighted and T2-weighted protocols. A TRUFI sequence was scanned to ensure that the materials could be visualized on ViewRay systems. Since FLAIR sequences are commonly used to enhanced lesions in the clinic, a FLAIR sequence was also used to compare the selected material's contrast.

Scanning sequence	T1-weighted gradient	TRUFI	T2-weighted gradient	FLAIR
FA	25°	70°	120°	120°
TR (ms)	9.5	4	3200	5000
TE (ms)	4.68	2	245	336
ETL	1	1	109	109
NEX	1	1	2	2

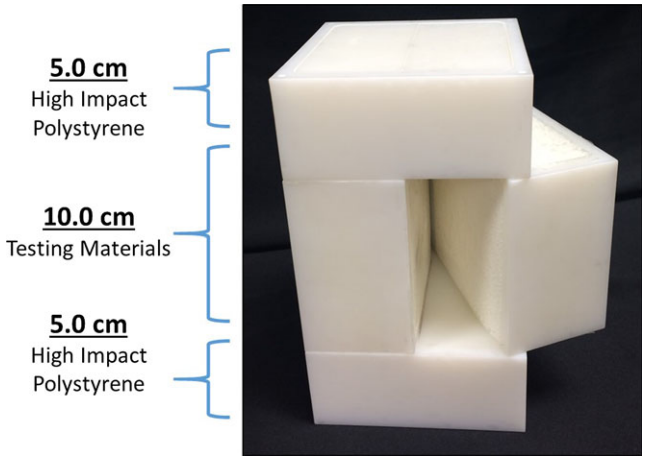

FIG. 2. PDD phantom was used to determine the testing material's dosimetric properties. The PDD phantom was divided into three subsections where the anterior and posterior sections were composed of polystyrene and the middle section was interchanged with testing materials. Film was placed in the sagittal plane to measure the material's PDD curve. [Color figure can be viewed at wileyonlinelibrarycom]

microdensitometer (Photoelectron Corporation, North Billerica, MA, USA) was used to capture the optical density of the film at the different depths of interest. The intensity of the film was then converted into dose and the dose at the varying depths was normalized to the dose at 1.5 cm.

3. RESULTS

3.A. MR properties

Most plastic, silicone, and gelatin-based materials tested were visible in both T1- and T2-weighted images. In-house mixtures were mostly visible on all four MR sequences. Specifically, testing materials that used either Polytek Development Corporation's Gel 25 or M-F Manufacturing Company's 100% Plastic Hardener were visible on T1-weighted images but were not visible on T2-weighted images. With few exceptions, most nylon, urethane, and epoxy-based materials were not visible on either T1- or T2-weighed MR sequences. Specifically, Smooth-On's Reoflex 20, Reoflex 30, VytalFlex 20, VytalFlex 30, and PMC 121/30 materials were all urethane-based and were only visible on T1-weighted images.

Materials that were heterogeneous and showed a random absence of signal were more favorable lung materials compared to the homogeneous substitutes since these materials were better representations of lung tissue. Heterogeneous-tested materials were constructed in-house, and were combined with a base material (either Sonneborn's petroleum jelly or Polytek Development Corporation's silicon gels) and different concentrations of 2–4 mm miniature Styrofoam balls. Within the heterogeneous lung materials, miniature Styrofoam balls represented air pockets with no MR signal while the surrounding base materials generated MR signal. MR visibility of potential lung equivalent materials greatly depended on the Styrofoam ball concentration. As the concentration of Styrofoam balls increased, the MR visibility greatly decreased since there was less signal from the surrounding materials. Among the in-house mixtures, the most visible lung substitute was a combination of 8.3% weight of Styrofoam balls and 91.7% of petroleum jelly (Fig. 3).

Contrary to potential lung candidates, homogeneous materials better represented soft tissue and tumor substitutes. Potential soft tissue and tumor substitutes were not required to have the same gray-scale contrast as their human flesh counterparts, but these materials were required to have visible contrast between water and each other. Taking into account all four MR sequences, three materials (Clear Ballistics' Gel #20, M-F Manufacturing Company's 100% Liquid PVC Plastic, and Radiation Products Design Incorporation's Superflab) were shown to have the most visible contrast between water, each other and other testing materials. Therefore, Gel #20, 100% Liquid PVC Plastic and Superflab were chosen to be tested further as suitable soft tissue or tumor substitutes (Fig. 3).

3.B. CT properties

The testing materials' (listed in Table I) HU was measured from images acquired on GE's Lightspeed CT simulator. In general, homogeneous plastic, nylon, epoxy-based materials most resembled soft tissue and their HU's, ranging from, −29 to 65, 82 to 161, 63 to 72, respectively. Urethane-based materials showed a larger HU range of −45 to 78. Gelatin-based materials resembled more fatty-like tissues with HU's ranging from −164 to −175 whereas homogenous silicone materials resembled more contrast-enhanced soft tissue with HU's ranging from 185 to 319. In-house mixtures, that

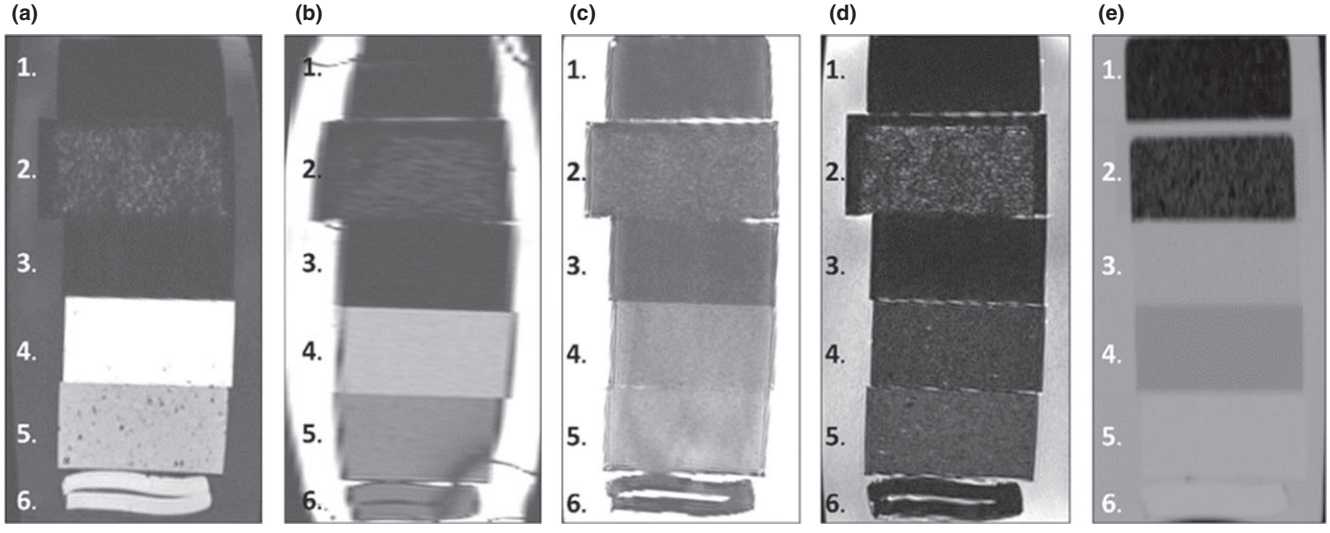

FIG. 3. From top to bottom, the materials shown are: 1.) compress cork, 2.) in-house petroleum/styrofoam mixture (8.3% weight composed of mini Styrofoam balls and 91.7% weight composed of Sonneborn's Petroleum jelly), 3.) polystyrene, 4.) Clear Ballistic Gel #20, 5.) M-F Manufacturing 100% liquid PVC plastic, and 6.) Superflab. Four different MR sequences (a–d) and a CT scan (e) were performed on these materials to visually determine their contrast between water and IROC-Houston's conventional materials. The MR sequences shown in this figure were a (a.) T1-weighted, (b.), TRUFI, (c.) T2-weighted, and (d.) fluid-attenuated T2-weighted scans. The HU measured from the CT image for compress cork, in-house petroleum/styrofoam mixture, polystyrene, Clear Ballistic Gel #20, Liquid plastic, and Superflab were, respectively, −800, −685, −33, −160, 20, and 51.

incorporated either silicone- or hydrocarbon-based materials, visually and numerically simulated lung-like materials with HU's that ranged from, −978 to −117 and −667 to −593, respectively. Similar to MR, the concentration of the Styrofoam balls directly affect their attenuation coefficient. Mixtures with greater Styrofoam ball concentrations had more air pockets which, enable the synthetic materials to better visually resembled lung tissue and had lower HU values.

The four selected MR-visible materials were collectively imaged on GE's Lightspeed CT simulator and are displayed in Fig. 3(e). Among the four selected MR-visible materials 100% Liquid PVC Plastic, and Superflab numerically represented soft tissue with HU of −10.4, and 59.9, respectively. Visually, the 100% Liquid PVC Plastic and Superflab materials had similar contrast as water, whereas Gel #20, showed a greater contrast relative to water and had a lower HU value of −170. Clear Ballistics' Gel #20 could potentially be used as either a fat or a tumor equivalent material since it did have lower HU value than water. Small fluctuations between mini Styrofoam balls and surrounding based materials in the heterogeneous mixtures created random signals that resemble high and low contrast areas. These random signals seen among in-house heterogeneous mixtures on a MR image were also comparable to random signal seen in lung tissue on a CT image. The in-house mixture with compositions of 8.3% of Styrofoam balls and 91.7% of petroleum jelly (which was previously selected as a potential synthetic lung substitute in MR) numerically resembled synthetic lung tissue with a HU of −685.

3.C. Dosimetric properties

The selected MR/CT-visible materials (in-house 91.7%/8.3% petroleum jelly/styrofoam mixture, Clear Ballistic Gel #20, and Liquid PVC Plastic) were further dosimetrically investigated. Since Superflab is currently used in the clinic as a tissue equivalent material, it was excluded from dosimetric measurement. Each selected material was irradiated under three different field sizes, then corresponding PDD curves were generated using the data from the TPS and radiochromic film. From a depth of 1.5 cm to 17 cm, the deviations between the film PDD and TPS PDD curves were determined for 10×10 cm^2, 6×6 cm^2, and 3×3 cm^2 field sizes. The greatest deviation between film and TPS PDD curves was found for the smallest field size for all materials. At a field size of 3×3 cm^2 the maximum deviation was: 12.2% at 17.0 cm for compress cork, 10.8% at 16.5 cm for the in-house petroleum jelly styrofoam mixture, 7.1% at 16.5 cm for polystyrene, 4.1% at 12.5 cm for Gel #20, and 4.6% at 17.0 cm for 100% Liquid PVC Plastic (Table III). While the greatest deviation between film and TPS PDD was shown for the 3×3 cm^2 field size, the average deviation for the 3×3 cm^2 field size for all of the materials was less than 6%. The mean deviation between film PDD and TPS PDD for the selected materials for the 10×10 cm^2 and 6×6 cm^2 field sizes were all less than 1.9%, and 2.8%, respectively. Quantitatively, the mean deviation for a 3×3 cm^2 field size the mean deviation for compress cork, the in-house petroleum jelly styrofoam mixture, polystyrene, Gel #20, and Liquid PVC Plastics were: 3.8 ± 3.60 cm, 5.9 ± 2.75 cm, 1.9 ± 2.02 cm, 1.5 ± 1.15 cm, and 2.0 ± 1.13 cm, respectively. At a field size of 3×3 cm^2, the maximum deviation was: 12.2% at 17.0 cm for compress cork, 10.8% at 16.5 cm for, 7.1% at 16.5 cm for polystyrene, 4.1% at 12.5 cm for Gel #20, and 4.6% at 17.0 cm for 100% Liquid PVC Plastic (Table III).

In addition to quantifying the maximum deviation between the film PDD and TPS PDD for each of the selected materials, the general shape of the tested material's PDD curves was compared with PDD curves of current IROC-Houston's lung and soft tissue equivalent materials. The in-house petroleum jelly/styrofoam mixture was compared to compress cork, which is commonly used as IROC-Houston's lung equivalent materials. Similarly, Gel #20, 100% Liquid PVC Plastic were compared to polystyrene, which is also commonly used as IROC-Houston's soft tissue equivalent materials. Collective PDD data for soft tissue and lung equivalent materials for the smallest (3×3 cm^2) and largest (10×10 cm^2) field sizes are shown in Fig. 4. Overall, the general PDD curve for Gel #20, and 100% Liquid PVC Plastic agreed with the polystyrene curve and the in-house petroleum/styrofoam mixture was in agreement with the compress cork curve. While modest discrepancies between general curve shapes between compress cork and the in-house heterogeneous mixture were seen in all three field sizes, the 3×3 cm^2 PDD curve showed a slightly higher deviation around 16 cm, where the lung-to-tissue interface was located. The PDD phantom's CT, which was used in the TPS, was not image with film sandwich in between the two halves. Therefore, it is believed that the higher deviation between the film and TPS measure in the smallest field size was primarily due to the dose build up from the film. Additionally, the petroleum/styrofoam mixture had a slightly higher physical density than compressed cork, which translated to having a smaller charge particle disequilibrium than compressed cork.

4. DISCUSSION

The materials selected for MRgRT end-to-end QA phantoms for IROC-Houston were based off of three major criteria: practicality, reliability, and accuracy. Since IROC-Houston credentials radiotherapy modalities by regularly shipping end-to-end QA phantoms to institutions, materials selected for a MR/CT-visible phantom needed to share practical characteristics that would ensure the phantom's shape and size remain constant over time. Materials that do not require specific shipping or storage conditions (i.e., could be left in room temperature, and insensitive to light) and show relative ease in constructing abnormal shapes were considered as practical materials. Prior to testing a material's imaging and dosimetric properties, the material's melting point was first investigated. The material's melting point was used to determine whether a material could withstand extreme temperatures during shipment. The highest temperatures a package

TABLE III. A measured film PDD curve and a TPS PDD curve were generated for both current IROC-Houston's phantom materials and testing materials for a large (10 × 10 cm^2), medium (6 × 6 cm^2), and small (3 × 3 cm^2) field size. For each material (compress cork, petroleum/Styrofoam mixture, polystyrene, Clear Ballistic Gel #20, and M-F manufacture's liquid PVC plastic), the maximum deviation between the material's measured PDD and TPS PDD and the overall mean deviation between 0.5 cm to 17 cm were recorded.

	10 × 10 cm^2			6 × 6 cm^2			3 × 3 cm^2		
Materials	Maximum deviation	Depth (cm)	Mean deviation	Maximum deviation	Depth (cm)	Mean deviation	Maximum deviation	Depth (cm)	Mean deviation
Compress cork	4.3	8.5	1.9 ± 1.12	5.1	15.5	2.0 ± 1.24	12.2	17.0	3.8 ± 3.60
Petroleum/styrofoam mix	7.7	15.0	1.9 ± 2.04	7.2	13.5	2.8 ± 2.26	10.8	16.5	5.9 ± 2.75
Polystyrene	5.7	17.0	1.8 ± 1.67	2.5	16.0	1.1 ± 0.59	7.1	16.5	1.9 ± 2.02
Clear ballistic Gel #20	1.9	15.0	0.6 ± 0.46	3.3	14.5	1.2 ± 0.81	4.1	12.5	1.5 ± 1.15
M-F manufacture liquid PVC plastic	3.7	16.5	1.2 ± 1.03	4.5	11.0	1.7 ± 1.21	4.6	17.0	2.0 ± 1.13

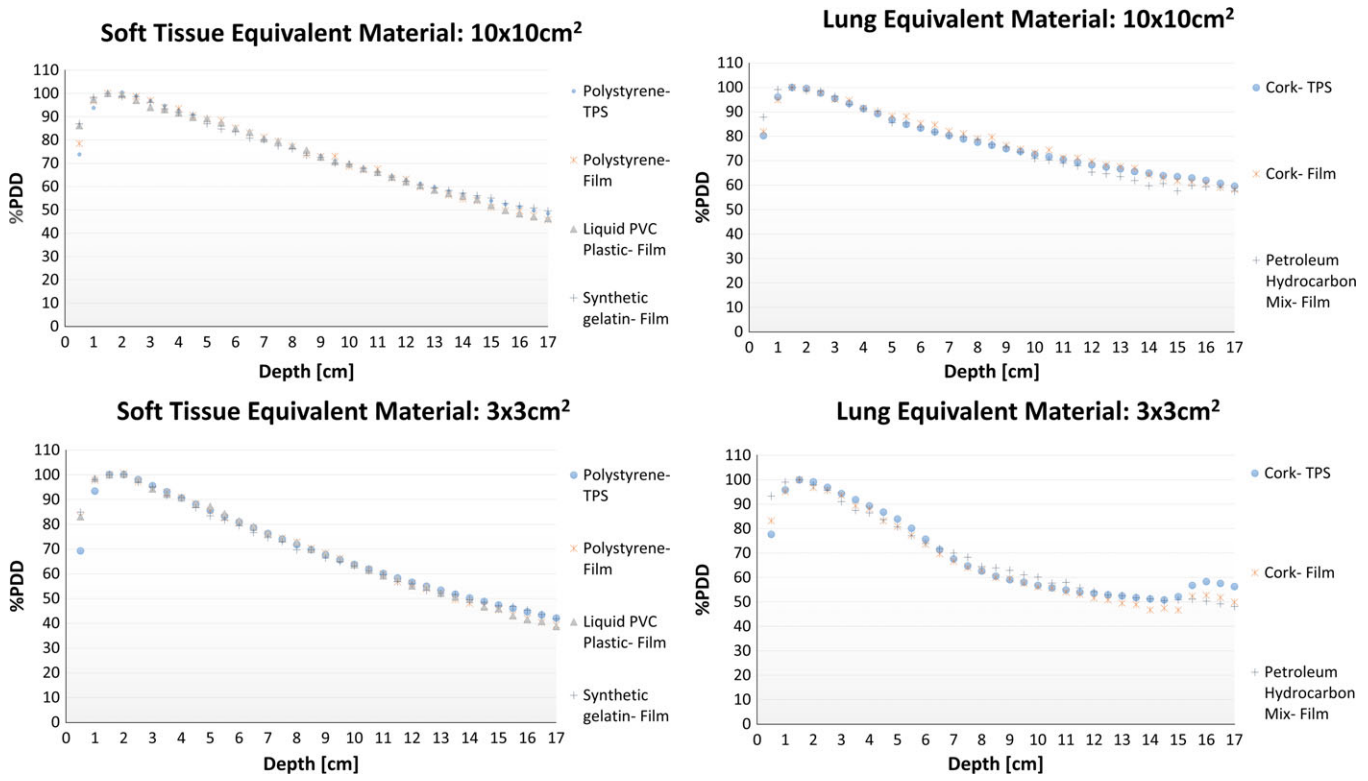

FIG. 4. The four graphs are a summary of the PDD curve comparisons between IROC-Houston's current soft tissue and lung equivalent materials and testing materials for a large (10 × 10 cm^2) and small (3 × 3 cm^2) field size. The interfaces between the testing materials and polystyrene of the PDD phantom occur between 5 cm and 15 cm. All graphs show the current tissue substitute's film (red) and treatment planning (blue) PDD curves. The testing materials were then compared to current tissue's film and TPS PDD curves. The greatest curve deviation occurs for the lung equivalent material for the small field size. [Color figure can be viewed at wileyonlinelibrarycom]

may experience for domestic and international shipments are, respectively, 37.1°C and 45.5°C.[19] Therefore, it was important that potential candidates had melting points greater than 45.5°C. Specifically, the melting points for: Superflab, in-house petroleum jelly styrofoam mixture, Gel #20, and Liquid PVC Plastics were: 93.3°C, 58.0°C, 92.2°C, and 121.1°C, respectively. The material's selection process was also judged based off of the material's reliability. Since IROC-Houston's QA phantoms are used for many years, the material's shape and consistency must remain constant over time (i.e., the materials must not deteriorate or dehydrate over time). The materials listed in Table I were tested for their reliability by sitting in room temperature for 3 months. All materials except for Clear Ballistics' Gel #4 and SuperStuff showed no forms of degradation. In addition to the practicality and reliability requirements, the materials selected for a MRgRT phantom had to be visible in common MR sequences, show comparable HU, and dosimetrically mimic their respective organ site.

Previously reported MR/CT-visible materials in the literature did not meet IROC-Houston's criteria since most of these materials shared short shelf lives and required refrigeration storage.[14–16] We tested over 80 materials, which could potentially be used to manufacture IROC-Houston's MRgRT

anthropomorphic phantoms. Most of the test materials shared comparable HU values as human tissue but were not visible on both T1- and T2-weighted MR images. Materials that were classified as either epoxy, urethane, or nylon-based sometimes showed contrast in T1-weighted images, but were consistently not visible in T2-weighted images. Either Polytek's silicone-based gels or Sonneborn's petroleum jelly was mixed with miniature Styrofoam balls in attempts to create various lung equivalent materials. Styrofoam balls were used to more realistically resemble a lung's heterogeneous appearance as viewed in MR and CT, and to lower the HU value. As we increased the concentration of Styrofoam balls, it created a more realistic lung attenuation coefficient, but consequently, became less visible in MR images. The in-house mixture of 8.3% Styrofoam balls and 91.7% petroleum jelly was selected as the most optimal material for a dual modality since it was a good compromised between MR image visibility and typical lung attenuation data.

Other promising MR/CT-visible materials were Smooth-On's Dragon Skin 30, Smooth-On's EcoFlex 50, and in-house mixtures composed of different concentration of Polytek's Gel 00 and miniature styrofoam balls. These materials were further investigated for their dosimetric properties, but are not displayed in Fig. 4 since these materials: (a) had higher physical density than their respective organ sites, and (b) did not have good dosimetric properties.

The selected testing materials visually showed different contrast among the four MR scans. However, among the scans, TRUFI showed the smallest contrast between the selected MR-visible materials. All materials were imaged using a magnetic field of 1.5 T. Using a smaller magnetic field (i.e., 0.35 T) would generate a smaller net magnetic moment, which would consequently lower SNR. Lowering the magnetic field strength could change the material's T1 and T2 relaxation times which would consequently effect the MR contrast. In order to predict the contrast in a lower magnetic field, the material's T1 and T2 relaxations times would need to be calculated.

The measured PDD curves for the selected materials were comparable with their predicted PDD curves. The general PDD shape of IROC-Houston's typical soft tissue substitute, polystyrene, was most comparable to measured PDD curves of Clear Ballistics' Gel #20, and 100% Liquid PVC Plastic. Similarly, the general PDD curve shape of IROC-Houston's conventional lung equivalent material, compress cork, was comparable to the in-house styrofoam/petroleum jelly mixture's measured PDD curve. Soft tissue equivalent materials showed a closer PDD curve agreement than lung equivalent materials. While all PDDs showed expected curve shapes, small differences were only noted for the smallest field size (3×3 cm^2) between the testing materials' measured and predicted PDD curves.

5. CONCLUSION

It was determined that four testing materials were visible and distinguishable in both MR and CT and dosimetrically represent human tissue. The in-house 91.7% petroleum jelly/8.3% styrofoam ball mixture resembled lung tissue since its HU was −685, dosimetrically showed expect lung equivalent PDD curves, and visually showed random signal in both modalities. Superflab is currently used in the clinics as a tissue equivalent bolus, so it was only visually examined. It was determined as a potential material to use in a MR/CT-visible phantom, since Superflab was visible in both imaging modalities. Lastly, Clear Ballistics' Gel #20 and 100% Liquid PVC Plastic were determined to dosimetrically represent soft tissue, and were easily viewed in both MR and CT modalities and it was therefore determined that both Clear Ballistics' Gel #20 and 100% Liquid PVC Plastic are possible tumor equivalent substitutes for MRgRT end-to-end QA phantoms.

ACKNOWLEDGMENTS

This work was supported by Public Health Service Grant U24 CA180803 awarded by the National Cancer Institute, United States Department of Health and Human Services. Additionally, this research is supported by the Andrew Sabin Family Foundation; Dr. Fuller is a Sabin Family Foundation Fellow.

CONFLICT OF INTEREST

None.

[a]Author to whom correspondence should be addressed Electronic mail: asteinmann@mdanderson.org; Telephone: 713-745-8989.

REFERENCES

1. Lecchi M, Fossati P, Elisei F, Orecchia R, Lucignani G. Current concepts on imaging in radiotherapy. *Eur J Nucl Med Mol Imaging*. 2008;35:821–837.
2. Bol GH, Lagendijk JJ, Raaymakers BW. Compensating for the impact of non-stationary spherical air cavities on IMRT dose delivery in transverse magnetic fields. *Phys Med Biol*. 2015;60:755–768.
3. Arumugam S, Sidhom M, Truant D, Xing A, Udovitch M, Holloway L. Variable angle stereo imaging for rapid patient position correction in an in-house real-time position monitoring system. *Phys Med*. 2017;33:170–178.
4. Fallone BG. The rotating biplanar linac-magnetic resonance imaging system. *Semin Radiat Oncol*. 2014;24:200–202.
5. Jaffray DA, Carlone MC, Milosevic MF, et al. A facility for magnetic resonance-guided radiation therapy. *Semin Radiat Oncol*. 2014;24:193–195.
6. Lagendijk JJ, Raaymakers BW, van Vulpen M. The magnetic resonance imaging-linac system. *Semin Radiat Oncol*. 2014;24:207–209.
7. Mutic S, Dempsey JF. The ViewRay system: magnetic resonance-guided and controlled radiotherapy. *Semin Radiat Oncol*. 2014;24:196–199.
8. Prior P, Chen X, Botros M, et al. MRI-based IMRT planning for MR-linac: comparison between CT- and MRI-based plans for pancreatic and prostate cancers. *Phys Med Biol*. 2016;61:3819–3842.
9. Brock KK, Dawson LA. Point: principles of magnetic resonance imaging integration in a computed tomography-based radiotherapy workflow. *Semin Radiat Oncol*. 2014;24:169–174.
10. Paulson ES, Erickson B, Schultz C, Allen Li X. Comprehensive MRI simulation methodology using a dedicated MRI scanner in radiation oncology for external beam radiation treatment planning. *Med Phys*. 2015;42:28–39.
11. Nyholm T, Jonsson J. Counterpoint: opportunities and challenges of a magnetic resonance imaging-only radiotherapy work flow. *Semin Radiat Oncol*. 2014;24:175–180.

12. Torresin A, Brambilla MG, Monti AF, et al. Review of potential improvements using MRI in the radiotherapy workflow. *Z Med Phys*. 2015;25:210–220.
13. Liney GP, Moerland MA. Magnetic resonance imaging acquisition techniques for radiotherapy planning. *Semin Radiat Oncol*. 2014;24:160–168.
14. Ruschin M, Davidson SR, Phounsy W, et al. Technical note: multipurpose CT, ultrasound, and MRI breast phantom for use in radiotherapy and minimally invasive interventions. *Med Phys*. 2016;43:2508.
15. Gallas RR, Hunemohr N, Runz A, Niebuhr NI, Jakel O, Greilich S. An anthropomorphic multimodality (CT/MRI) head phantom prototype for end-to-end tests in ion radiotherapy. *Z Med Phys*. 2015;25:391–399.
16. Niebuhr NI, Johnen W, Guldaglar T, et al. Technical note: radiological properties of tissue surrogates used in a multimodality deformable pelvic phantom for MR-guided radiotherapy. *Med Phys*. 2016;43:908–916.
17. Followill DS, Evans DR, Cherry C, et al. Design, development, and implementation of the radiological physics center's pelvis and thorax anthropomorphic quality assurance phantoms. *Med Phys*. 2007;34:2070–2076.
18. Molineu A, Followill DS, Balter PA, et al. Design and implementation of an anthropomorphic quality assurance phantom for intensity-modulated radiation therapy for the Radiation Therapy Oncology Group. *Int J Radiat Oncol Biol Phys*. 2005;63:577–583.
19. Singh SP, Singh J, Saha K. Measurement and analysis of physical and climatic distribution environment for air package shipment. *Packag Technol Sci*. 2015;28:719–731.